

# Particle number conservation in quantum many-body simulations with matrix product operators

**Dominik Muth**<sup>1,2</sup>

<sup>1</sup> Fachbereich Physik und Forschungszentrum OPTIMAS, Technische Universität Kaiserslautern, Erwin-Schrödinger-Str. 46, D-67663 Kaiserslautern

<sup>2</sup> Graduiertenschule Materials Science in Mainz, Technische Universität Kaiserslautern, Erwin-Schrödinger-Str. 46, D-67663 Kaiserslautern

E-mail: [muth@physik.uni-kl.de](mailto:muth@physik.uni-kl.de)

**Abstract.** Incorporating conservation laws explicitly into Matrix product states (MPS) has proven to make numerical simulations of quantum many-body systems much less resources consuming. We will discuss here, to what extent this concept can be used in matrix product operators (MPO). Quite counter-intuitively the expectation of gaining in speed by sacrificing information about all but a single symmetry sector is not in all cases fulfilled. It turns out that often the entanglement imposed by the global constraint of fixed particle number is the limiting factor in the canonical ensemble.

PACS numbers: 02.70.-c, 05.10.Cc, 05.30.-d, 05.50.+q,

## 1. Introduction

Variational MPS methods have been used for more than half a century<sup>1</sup> to describe the transfer matrix of two-dimensional classical models in statistical mechanics, which are equivalent to one-dimensional quantum systems. For references see, e.g., the work of Baxter<sup>2</sup> and references therein. Later on the density-matrix renormalisation group (DMRG) method<sup>3</sup> has been developed independently and proved very successful in describing low-energy eigenstates of one-dimensional quantum lattice systems which are typically only moderately entangled. In the last decade DMRG has been extended to real-time evolution<sup>4-7</sup> (t-DMRG). These and various extended implementations all rely on the MPS framework to capture the relevant part of the Hilbert space in terms of the largest singular values.<sup>8,9</sup>

Conservation laws resulting from global symmetries can be taken into account explicitly in the construction of MPSs.<sup>8,10</sup> This reduces the local Hilbert space dimension such that approximations with higher matrix dimensions can be calculated using the same amount of computation time and memory. In addition arithmetical errors of the type that would lead out of the symmetry sector of the initial state are impossible. Particle number conservation is present in many non-relativistic model systems and implemented in MPS algorithms routinely.<sup>11</sup> Its explicit implementation is necessary if one wants to calculate dynamical properties in the low filling limit,<sup>12,13</sup> where the average number of particles per lattice site is small compared to 1, as it results e.g. from the discretization of a continuous model.<sup>14</sup>

In DMRG like dynamical simulations matrix product *operators* naturally arise either as density-operators at non-zero-temperature<sup>15,16</sup> or in open systems<sup>15-18</sup> or as general operators in the Heisenberg picture.<sup>19</sup> It has been demonstrated recently, that the scaling of the entanglement entropy with time in the Heisenberg picture can be much more favourable than in the Schrödinger picture in the presence of a conservation law.<sup>20</sup>

Let us assume that we want to do a Heisenberg picture calculation. There exist two distinct ways of imposing a symmetry onto MPOs. For simplicity we will restrict the discussion to particle number conservation. The first option reduces the Hilbert space dimension only halfway, as the operator is not projected onto a certain symmetry sector. This approach has already proven useful in practical calculations<sup>20</sup> and introduces no entanglement overhead. The second option reduces the Hilbert space further by projecting onto a symmetry sector. This approach however introduces additional entanglement in the initial MPO. If the filling is sufficiently low this is not a problem. However it can make the method less useful in the generic case.

In the Heisenberg picture the space of operators can be mapped to a “super-space” of kets via

$$\hat{O} = \sum_{\vec{i}, \vec{j}} o_{\vec{i}, \vec{j}} |\vec{i}\rangle \langle \vec{j}| \longmapsto |\hat{O}\rangle = \sum_{\vec{i}, \vec{j}} o_{\vec{i}, \vec{j}} \left| \begin{array}{c} \vec{j} \\ \vec{i} \end{array} \right\rangle. \quad (1)$$

Here the  $\vec{i}$  and  $\vec{j}$  are vectors of occupation numbers for every lattice site, thus corresponding to a Fock state. In these terms we talk about an upper in- and a lower out-chain. (“In” and “out” refer to the original operator acting as a function.) An MPO is then equivalent to an MPS

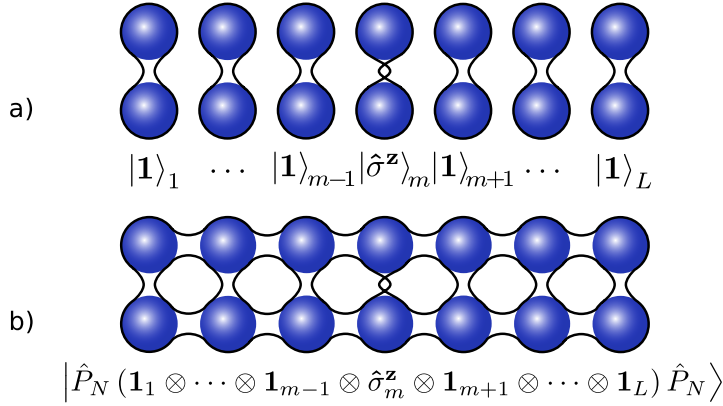


**Figure 1.** a) In the grand canonical Hilbert space a product operator can be interpreted as a state on a double chain, which can be in general maximally entangled locally, but not at all along the chain. b) If the operator is however projected to a certain symmetry sector, the corresponding double-chain state gets entangled also along the chain. This entanglement can overcompensate the benefits from shrinking the Hilbert space, depending on the symmetry sector in question.

representation of such a “super-state”. Given the canonical<sup>21</sup> form of the MPS<sup>‡</sup>, the Schmidt decomposition at two neighbouring bonds reads

$$|\hat{O}\rangle = \sum_{\alpha,\beta=1}^{\chi} \sum_{i=0}^{d-1} \sum_{j=0}^{d-1} \lambda_{\alpha}^{[m-1]} \Gamma_{\alpha,\beta}^{[m]i,j} \lambda_{\beta}^{[m]} \left| \begin{matrix} j \\ i \end{matrix} \right\rangle_m \otimes |\alpha\rangle_{\mathbf{A}} \otimes |\beta\rangle_{\mathbf{B}}. \quad (2)$$

The sub-chain A comprises sites 1 to  $m - 1$ , the sub-chain B comprises sites  $m$  to  $L$  where  $L$  is the total number of sites.  $\chi$  is the bond dimension of the MPS.

The first thing to notice is, that the  $\Gamma$  tensor has two physical indices  $i$  and  $j$ , one for each chain, and both take all possible values, 0 to  $d - 1$ , where  $d$  is the local dimension. It turns out, that this is an unnecessary overhead in the presence of a symmetry, and in the case of particle number conservation, we can eliminate either one or two of these indices completely. The latter option has the advantage, that we do not have to limit the local dimension explicitly to  $d$ , as one would have to do otherwise, e.g., for a bosonic model, but requires the projection of the operator onto a symmetry sector.

The other observation is that a product operator always maps to a product state, i.e., with bond dimension  $\chi = 1$ , and therefore with no entanglement between the sites:

$$\bigotimes_m \hat{O}^{[m]} = \bigotimes_m \left( \sum_{i,j} o_{j,i}^{[m]} |i\rangle_m \langle j|_m \right) \mapsto \bigotimes_m \left( \sum_{i,j} o_{j,i}^{[m]} \left| \begin{matrix} j \\ i \end{matrix} \right\rangle_m \right). \quad (3)$$

Product operators, and eventually sums of a small number of those, form the majority of physically interesting quantities. The fact that we find no entanglement in them in the first place, makes the Heisenberg picture a promising approach. If we project a product operator

<sup>‡</sup> In this context the word “canonical” refers to the orthogonality and normalisation properties of the Schmidt decomposition which we do not find in an MPS in its most general form. It is not to be mixed up with canonical in the sense of working at a fixed particle number, section 3.

to a given symmetry sector, it does not necessarily map onto a product state any more. This is illustrated in figure 1.

The Heisenberg equation of motion for the operators,  $i\partial_t \hat{O} = [\hat{O}, \hat{H}]$ , gives rise to a Schrödinger type equation of motion for the “super-states“,  $i\partial_t |\hat{O}\rangle = \tilde{H} |\hat{O}\rangle$ , with the new Hamiltonian

$$\tilde{H} = \mathbf{1} \otimes \hat{H} - \hat{H} \otimes \mathbf{1}. \quad (4)$$

Thus this “super-Hamiltonian” acts on the in- and out-chains independently. In general the dynamics is however not just the dynamics of two independent chains, because the initial operator will be mapped to a state with strong entanglement between in- and out-chain, equation (1). Again, if  $\hat{H}$  conserves the total particle number  $\hat{N} = \sum_m \hat{n}_m$ , i.e.,  $[\hat{N}, \hat{H}] = 0$ , there exist two different ways of imposing this onto the MPO. In sections 2 and 3 we will discuss them in detail. Section 4 will give details on how to construct the projected operator in practise and gives exact results on the entanglement overhead introduced. Section 5 gives example calculations, which illustrate how the two methods and also the brute force method, where no symmetry is taken into account, perform in comparison.

## 2. Unprojected operators

To introduce the first method we observe that  $\tilde{H}$  conserves the number *difference* between the in- and out- chains:

$$[\tilde{H}, \hat{N} \otimes \mathbf{1} - \mathbf{1} \otimes \hat{N}] = 0 \quad (5)$$

Thus, if we consider operators (more precisely: operators in the Heisenberg picture at  $t = 0$ ) which destroy or create a given number of particles (like, e.g., the particle annihilation and creation operators  $\hat{a}_m$  or  $\hat{a}_m^\dagger$  at some given site  $m$ , and products of those) they will map to an eigenstates of this difference. Note that the identity on the whole Hilbert space,

$$\mathbf{1} = \bigotimes_m \mathbf{1}^{[m]}, \quad (6)$$

is a prototype of such an operator. The dynamics will then take place only in a specific symmetry sector and the MPO can be restricted accordingly. This can be done in exactly the same way as for MPS when the total number itself is conserved:

Given the canonical<sup>21</sup> form of the MPS, the Schmidt decomposition at two neighbouring bonds then reads

$$|\hat{O}\rangle = \sum_{\alpha, \beta=1}^{\chi} \sum_{j=0}^{d-1} \lambda_{\alpha}^{[m-1]} \Gamma_{\alpha, \beta}^{[m]j} \lambda_{\beta}^{[m]} \left| \begin{matrix} j \\ i \end{matrix} \right\rangle_m \otimes |\alpha\rangle_{\mathbf{A}} \otimes |\beta\rangle_{\mathbf{B}}. \quad (7)$$

If  $|\hat{O}\rangle$  is a particle number difference eigenstate, then also the Schmidt vectors  $|\alpha\rangle_{\mathbf{A}}$  and  $|\beta\rangle_{\mathbf{B}}$  must be eigenstates of the particle number difference in their respective subsystems. The local particle number difference  $j - i$  is thus determined from  $j$ ,  $\alpha$  and  $\beta$  alone, and there is no second physical index  $i$  present in the  $\Gamma$  tensor, differently from (2). This particular form of the MPS can be kept during time evolution. For details we refer the reader to the

literature.<sup>8,10,11</sup> It should be noted at this point, that particle number conservation can in this way only be applied to an MPS for open boundary conditions. Periodic<sup>22</sup> or infinite<sup>23</sup> boundary conditions are excluded.

This method of using the conservation law for MPOs was used recently in<sup>20</sup> and gives great advantage over the plain approach which works for general systems without conservation laws. A comparison for an example case can be found in section 5.

Before we continue to the second method, we take a look at the entanglement in this first approach. Therefore we give an explicit construction of the initial MPO in two steps.

The first step is the construction of of an MPO for the identity. This task is trivial, but we take a route that can be conveniently generalised in section 3: Given a state  $\sum_{\vec{j}} c_{\vec{j}} |\vec{j}\rangle$ , that is a superposition of Fock states, the mapping

$$|j\rangle_m \mapsto |j\rangle_m \langle j|_m, \quad (8)$$

which is applied locally at every site  $m$  simultaneously, maps it to a superposition  $\sum_{\vec{j}} c_{\vec{j}} |\vec{j}\rangle \langle \vec{j}|$  of projectors onto these Fock states. We get the identity matrix by superimposing *all* Fock states with amplitude  $c_{\vec{j}} = 1$ ,

$$\sum_{\vec{j}} |\vec{j}\rangle \langle \vec{j}| = \bigotimes_m \left( \sum_{j=0}^{d-1} |j\rangle_m \langle j|_m \right) \mapsto \bigotimes_m \left( \sum_{j=0}^{d-1} |j\rangle_m \langle j|_m \right) = \sum_{\vec{j}} |\vec{j}\rangle \langle \vec{j}| = \mathbf{1}. \quad (9)$$

It's MPO representation,

$$\begin{aligned} |\mathbf{1}\rangle &= \sum_{\vec{j}} \left| \begin{smallmatrix} \vec{j} \\ \vec{j} \end{smallmatrix} \right\rangle = \bigotimes_m \left( \sum_{j=0}^{d-1} \left| \begin{smallmatrix} j \\ j \end{smallmatrix} \right\rangle_m \right) \\ &= \sum_{j_1, j_2, \dots, j_L=0}^{d-1} \Gamma^{[1]j_1} \Gamma^{[2]j_2} \dots \Gamma^{[L]j_L} \left| \begin{smallmatrix} j_1 \\ j_1 \end{smallmatrix} \right\rangle_1 \otimes \left| \begin{smallmatrix} j_2 \\ j_2 \end{smallmatrix} \right\rangle_2 \otimes \dots \otimes \left| \begin{smallmatrix} j_L \\ j_L \end{smallmatrix} \right\rangle_L, \end{aligned} \quad (10)$$

thus has large entanglement between the two chains. The entanglement is however contained *within* the matrices themselves. There is no entanglement between different lattice sites, thus a bond dimension of  $\chi = 1$  suffices. The bond indices  $\alpha$  and  $\beta$  therefor do not show up in (11) and the  $\Gamma$  tensors can be chosen to have entries of 1 everywhere.

In the second step we get the MPO representation of  $\hat{O}$  by applying  $\hat{O}$  itself only to the out-chain of  $|\mathbf{1}\rangle$ ,

$$|\hat{O}\rangle = \sum_{\vec{i}, \vec{j}} o_{\vec{i}, \vec{j}} \left| \begin{smallmatrix} \vec{j} \\ \vec{i} \end{smallmatrix} \right\rangle = \left( \mathbf{1} \otimes \hat{O} \right) |\mathbf{1}\rangle. \quad (12)$$

If  $\hat{O}$  is reasonably simple, then its MPO will also have a simple form. This will change dramatically however, if we project the operator to the subspace of a given particle number, as discussed in the next section.

### 3. Projected operators

$\tilde{H}$  does of course not only conserve the number difference between the two chains, but also the total numbers in each chain separately:

$$\left[ \tilde{H}, \hat{N} \otimes \mathbf{1} \right] = \left[ \tilde{H}, \mathbf{1} \otimes \hat{N} \right] = 0 \quad (13)$$

However MPO representations are in general not eigenstates of any of these. This also holds for product operators. Taking into account particle number conservation in each chain therefore only applies to operators that are nonzero only in a given symmetry sector. On the other hand any operator can be decomposed in the following way:

$$\hat{O} = \sum_{N,M} \hat{P}_M \hat{O} \hat{P}_N, \quad (14)$$

where  $\hat{P}_N$  and  $\hat{P}_M$  are the projectors onto the  $N$ - and  $M$ -particle Hilbert space. Thus if we project the operator to a given input and output particle number, we find an eigenstate of the total particle number in the upper *and* in the lower chain simultaneously. Particle number conservation can then be used twice:

The Schmidt decomposition at two neighbouring bonds now reads

$$|\hat{O}\rangle = \sum_{\alpha,\beta=1}^{\chi} \lambda_{\alpha}^{[m-1]} \Gamma_{\alpha,\beta}^{[m]} \lambda_{\beta}^{[m]} \left| \begin{matrix} j \\ i \end{matrix} \right\rangle_m \otimes |\alpha\rangle_{\mathbf{A}} \otimes |\beta\rangle_{\mathbf{B}}. \quad (15)$$

If  $|\hat{O}\rangle$  is a particle number eigenstate in both chains, then also the Schmidt vectors  $|\alpha\rangle_{\mathbf{A}}$  and  $|\beta\rangle_{\mathbf{B}}$  must be eigenstates of the particle number in both chains in their respective subsystems. The local particle numbers  $i$  and  $j$  are thus determined from  $\alpha$  and  $\beta$  alone, and there are no physical indices present in the  $\Gamma$  tensor anymore. This particular form of the MPS can again be kept during time evolution.

If the operator itself destroys (or creates) a given number of particles (14) simplifies to

$$\hat{O} = \sum_N \hat{P}_{N-n} \hat{O} \hat{P}_N, \quad (16)$$

where  $n$  is the number of particles destroyed. We get the MPO representation of  $\hat{P}_{N-n} \hat{O} \hat{P}_N$  by applying  $\hat{O}$  itself to the out-chain of the MPO representation of  $\hat{P}_N$ ,

$$|\hat{P}_{N-n} \hat{O} \hat{P}_N\rangle = \left( \mathbf{1} \otimes \hat{O} \right) |\hat{P}_N\rangle. \quad (17)$$

$\hat{P}_N$  is now the identity *only in the sector of particle number  $N$* . It vanishes in the remains of the grand canonical Hilbert space.  $\hat{P}_N$  takes the role as a prototype of a projected operator, analogous to unity in (12). The difficulty of the second approach results from the fact that  $\hat{P}_N$  is clearly not a product operator, but entangled between the sites, as illustrated in figure 1. We will construct it explicitly in section 4.

Of course  $\hat{O}$  and  $\hat{P}_{N-n} \hat{O} \hat{P}_N$  are not equivalent. But in certain cases this is not relevant, e.g. if  $\hat{O}$  is an observable (which implies  $n = 0$ ), and we evolve  $\hat{O}$  in time using Heisenberg t-DMRG in order to find the dynamics of its expectation value. Then the result is the same

using  $\hat{P}_N \hat{O} \hat{P}_N$  if the state  $|\Psi_0\rangle$  of the system for which we want to calculate the expectation value is a particle number eigenstate,  $\hat{N} |\Psi_0\rangle = N |\Psi_0\rangle$ :

$$\langle \Psi_0 | \hat{O}_t | \Psi_0 \rangle = \langle \Psi_0 | \hat{P}_N \hat{O}_t \hat{P}_N | \Psi_0 \rangle = \langle \Psi_0 | \left( \hat{P}_N \hat{O} \hat{P}_N \right)_t | \Psi_0 \rangle \quad (18)$$

An example of this type is given for a bosonic model at the end of section 5.

#### 4. Preparing the projector onto the subspace of a fixed particle number

What is left is the construction of  $|\hat{P}_N\rangle$ . Following the arguments in section 2 for the construction of  $|1\rangle$ , this reduces to preparing an MPS that is a superposition of all Fock states *with total particle number  $N$* , which will be discussed in the following. The operationally simple mapping (8) together with (1) will transform it to  $|\hat{P}_N\rangle$ .

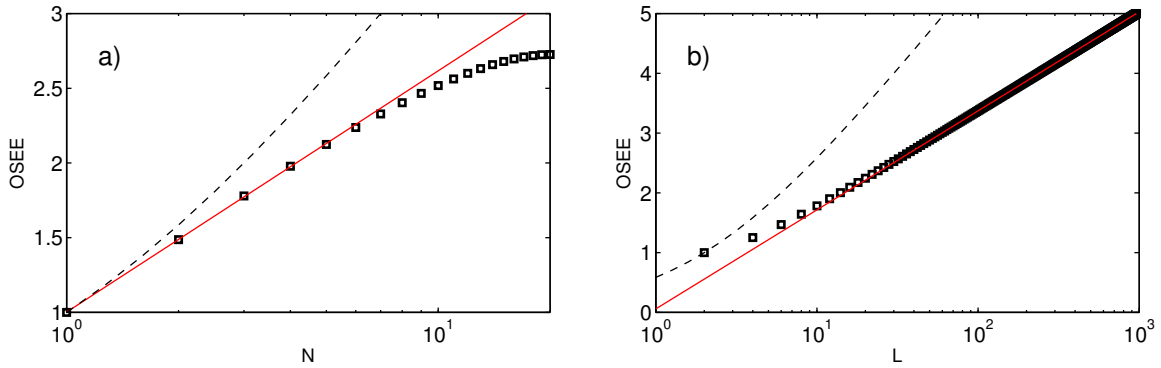


**Figure 2.** Logarithmic scaling of the OSEE of the projector  $\hat{P}_N$  at the centre of the chain with particle number  $N$  and system size  $L$ . We show  $S^{[L/2]}$  in a system of fermions ( $d = 2$ ) on a lattice, a) as a function of  $N$  for fixed system size  $L = 40$ . (Note that as  $N > L/2$  the entropy goes down again due to the Pauli principle and particle hole symmetry.) b) as a function of  $L$  for a fixed filling of  $N/L = 1/2$ . – Symbols are from the numerical evaluation of (20). Straight lines show fits to these. Dashed lines show the upper limit (26). We checked numerically, that also for a higher local dimension  $d$  the prefactor of the logarithmic scaling actually stays much below this limit.

Let us denote the normalised, equal superposition of all  $N$ -particle Fock states which are locally constrained to a maximum particle number of  $d - 1$  by  $|N\rangle$ . If we want to work without a local constraint, we set  $d = N + 1$ . Given a bi-partition of our lattice we note that its Schmidt decomposition is

$$|N\rangle = \sum_{l=0}^N \lambda_l^{[m]} |l\rangle_A \otimes |N-l\rangle_B. \quad (19)$$

The sub-chain A comprises sites 1 to  $m$ , the sub-chain B comprises sites  $m + 1$  to  $L$ . This shows that the MPS will have bond dimension  $\chi = N + 1$ .  $\lambda_l^{[m]^2}$  is the probability of finding  $l$  particles left of bond  $m$ :

$$\lambda_l^{[m]^2} = \frac{\Omega_d(l, m) \Omega_d(N-l, L-m)}{\Omega_d(N, L)}. \quad (20)$$

Here  $\Omega_d(n, L)$  is the number of possibilities to distribute  $n$  indistinguishable particles among  $L$  sites in such a way that no site is occupied by more than  $d - 1$  particles, given by the recursion formula<sup>24</sup>

$$\Omega_d(n, L) = \sum_{j=0}^{\min(n, d-1)} \Omega_d(n-j, L-1); \quad \Omega_d(n, 0) = \delta_{n0}. \quad (21)$$

For  $d = 2$  this reduces to  $\Omega_2(n, L) = \binom{L}{n}$ , for  $d > n$  it reduces to  $\Omega_{d>n}(n, L) = \binom{L+n-1}{n}$ .

We continue with the Schmidt decomposition at the following bond. (Repeating it for all bonds leads to the canonical form of the MPS.) Here the remaining task is to determine the coefficients of

$$|N\rangle = \sum_{l=0}^N \sum_{r=0}^N \lambda_l^{[m]} \Gamma_{lr}^{[m+1]} \lambda_r^{[m+1]} |l\rangle_{\mathbf{A}} \otimes |r-l\rangle_{m+1} \otimes |N-r\rangle_{\mathbf{B}'}. \quad (22)$$

The  $\lambda$  tensors are already known from (20). The sub-chain  $\mathbf{B}'$  comprises sites  $m+2$  to  $L$ . Thus  $\Gamma_{lr}^{[m+1]^2} \lambda_r^{[m+1]^2}$  is the probability of finding  $N-r$  particles at the right side of bond  $m+1$  provided that there are already  $l$  particles at the left of bond  $m$ :

$$\begin{aligned} \Gamma_{lr}^{[m+1]^2} \lambda_r^{[m+1]^2} &= \frac{\Omega_d(r-l, 1) \Omega_d(N-(r-l), L-1)}{\Omega_d(N, L)} \times \\ &\times \frac{\Omega_d(l, m) \Omega_d(N-r, L-m-1)}{\Omega_d(N-(r-l), L-1)} \times \frac{1}{\lambda_l^{[m]^2}}. \end{aligned} \quad (23)$$

Equations (20) and (23) determine the  $\Gamma$  and  $\lambda$  tensors completely. Thus we can calculate the coefficients of the MPS exactly. By means of (8) and (1) this also yields the MPO representation of  $\hat{P}_N$ :

$$|N\rangle \xrightarrow{(8)} \frac{\hat{P}_N}{\sqrt{\Omega_d(N, L)}} \xrightarrow{(1)} \frac{|\hat{P}_N\rangle}{\sqrt{\Omega_d(N, L)}}. \quad (24)$$

The  $\Gamma$  matrices do not have physical indices explicitly, because the local particle numbers are given by the bond indices (due to particle number conservation),  $l$  and  $r$  here. Note that in this particular case, the value of the bond index has a physical meaning, namely the particle number at the left side of the bond  $m$  considered. The absence of physical indices is especially useful for bosonic systems. There we can easily set  $d = N + 1$  without any overhead in memory. Thus we gain access to the dynamics of the locally unbounded system, while we would have to truncate the local Hilbert space in the grand-canonical case.

This construction shows the main difficulty of going to the canonical version of the MPO: Even the trivial operator  $\mathbf{1}$  has an extensive bond dimension of  $\chi = N + 1$  if projected to a fixed particle number  $N$ . The initial entanglement, even of a local operator, is no longer only between the chains but also along the chain, see the illustration in figure 1 and the example in figure 4. Although computations can be done with a higher bond dimension here, this



advantage is often overcompensated by the initial entanglement. However a linear growth of the matrix dimension does not imply, that the algorithm is inefficient. In contrast, the required matrix dimension in general grows exponentially with *time*,<sup>25</sup> which is a more severe limitation. Here, a linear scaling of the matrix dimension implies that the operator space entanglement entropy (OSEE)

$$S^{[m]} = - \sum_{\alpha=1}^x \lambda_{\alpha}^{[m]2} \log_2 \left( \lambda_{\alpha}^{[m]2} \right) \quad (25)$$

scales only logarithmically with system size,

$$S^{[m]} = - \sum_{l=0}^L \lambda_l^{[m]2} \log_2 \left( \lambda_l^{[m]2} \right) \leq \log_2(N + 1), \quad (26)$$

which is favourable§. In fact this upper bound is not even tight, as shown in figure 2. For details on the relation between the scaling of the entropy and the efficiency of an MPS see.<sup>27</sup>

## 5. Examples

As first example we take the spin- $\frac{1}{2}$  XXZ chain

$$\hat{H} = -\frac{1}{2} \sum_{\langle m,n \rangle} (\hat{\sigma}_m^x \hat{\sigma}_n^x + \hat{\sigma}_m^y \hat{\sigma}_n^y + \Delta \hat{\sigma}_m^z \hat{\sigma}_n^z), \quad (27)$$

where the  $\hat{\sigma}$  denote the Pauli matrices and the sum runs over all nearest neighbours. The U(1) symmetry (rotation around the z-axis) of the system implies conservation of the total magnetisation  $\hat{M}_z = \sum_m \hat{\sigma}_m^z$ . Via a Wigner-Jordan transformation this transforms into particle number conservation in the equivalent fermion lattice model.

The transport properties of the model depend strongly on the anisotropy  $\Delta$ . In the critical regime,  $|\Delta| < 1$ , transport is believed to be ballistic, while in the gapped regime it seems diffusive.<sup>18</sup> A quantity of interest in this context is the infinite temperature auto-correlation function (ITAC)

$$\langle \hat{O}_t^\dagger \hat{O} \rangle_{T=\infty} = \text{Tr} \left[ \hat{O}_t^\dagger \hat{O} \hat{\rho}_{T=\infty} \right] \quad (28)$$

for  $\hat{O} = \hat{\sigma}^z$  at a given lattice site. The expectation value is taken at infinite temperature, which makes it straight forward to calculate it from the Heisenberg picture time evolution||. It decays as  $t^{-1/2}$  in the case of diffusive and  $t^{-1}$  in the case of ballistic transport. However the asymptotics are hard to get numerically, especially for  $\Delta$  around 1 and larger. There exist

§ Actually the polynomial scaling of the matrix dimension can be taken as the definition of efficient. The nontrivial problem in general is to show that from the logarithmic scaling of the entanglement entropy one can conclude that there exist efficient approximations by MPS, see, e.g.<sup>26</sup>

|| Note that the infinite temperature density matrix of any system is proportional to the unity operator. Therefore from the definition of the ITAC, we see that in order to calculate it we have to do the same in the Schrödinger picture (take  $\text{Tr} \left[ \hat{O}^\dagger \cdot \hat{U}_t \hat{O} \mathbf{1} \hat{U}_t^\dagger \right]$ , where  $\hat{U}_t$  is the full propagator) and in the Heisenberg picture (take  $\text{Tr} \left[ \hat{U}_t^\dagger \hat{O}^\dagger \mathbf{1} \hat{U}_t \cdot \hat{O} \right]$ ). In fact this is an example where the requirement of using a mixed state in the Schrödinger picture makes it exactly as demanding as the Heisenberg picture calculation.

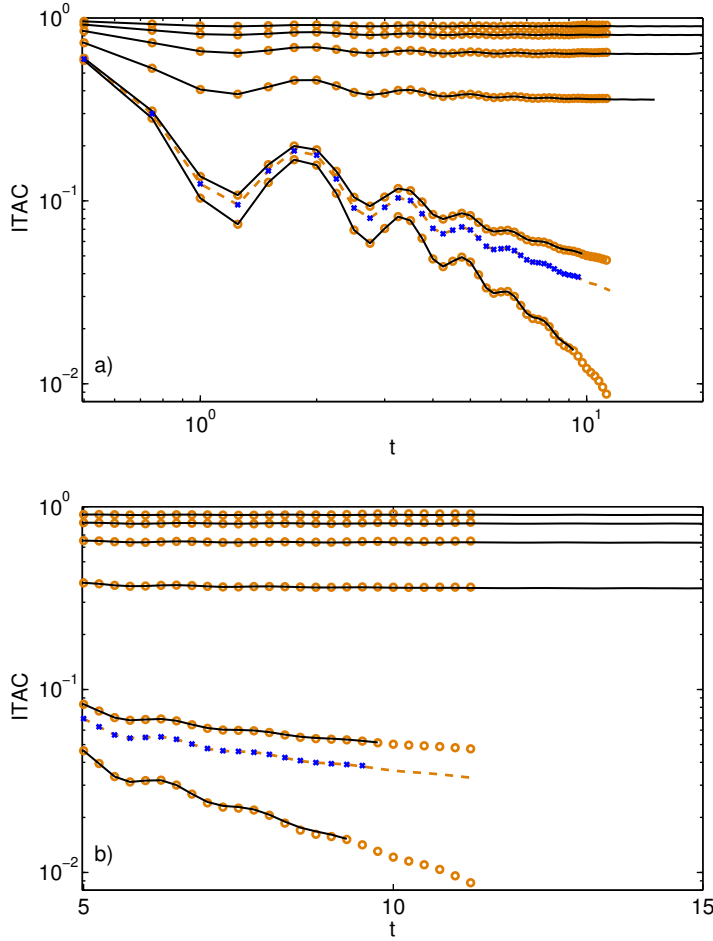


**Figure 3.** Spin- $\frac{1}{2}$  XXZ-chain of length  $L = 40$  at  $\Delta = 0.8$ , time evolution in the Heisenberg picture. ITAC at site  $m = 20$ :  $\Re[C_N(t)]$  ( $N = 1, 2, 4, 8, 16, 20$  from top down, calculated using the projected (solid line) and the unprojected method (orange circles)) and  $\Re[G(t)]$  calculated from the unprojected (dashed orange) and a brute force method (blue crosses) the latter ignoring particle number conservation completely. a) double logarithmic plot to emphasise the power law behaviour of the ITAC. b) same data as a), but linear time axis for better visibility of the difference in time reached by the different methods (and in the different symmetry sectors in case of the projected method). Bond dimensions used where  $\chi = 4000$  in the canonical calculations,  $\chi = 1000$  for the grand-canonical example, and  $\chi = 500$  in the brute force calculation. All curves end at the point where the accumulated cut-off error reaches  $10^{-2}$ . A TEBD<sup>4</sup> version of the t-DMRG algorithm is used with a fourth order trotter decomposition and time step size  $1/4$  in all cases. Curves are shown only up to  $t = 20$ . At later times boundary effects show up, because the excitations have propagated to the end of the chain.

exact diagonalization,<sup>28</sup> as well as transfer matrix DMRG<sup>29</sup> studies. The Heisenberg picture t-DMRG results using unprojected operators presented here reproduce the results of the latter. The timescale accessible with Heisenberg picture t-DMRG is somewhat larger. For the value of  $\Delta = 0.8$  we find an exponent for the decay of  $-0.83$  from the data shown in figure 3 using an empirical fitting function proposed in.<sup>28</sup> Although this value is slightly closer to  $-1$  than in

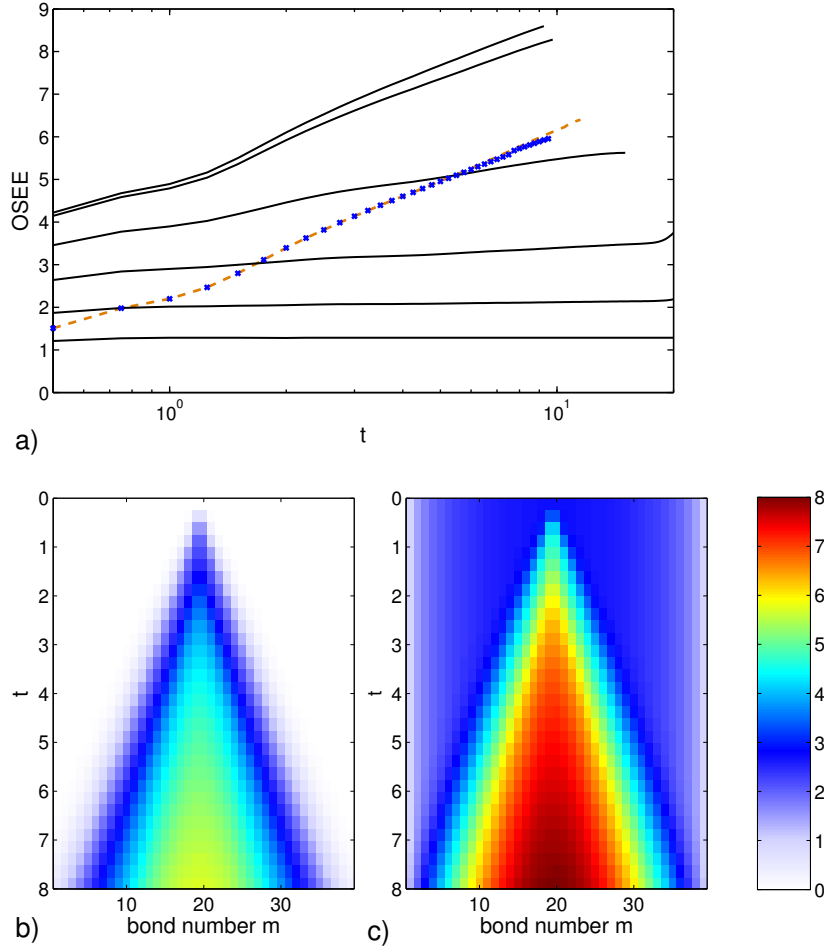


**Figure 4.** Spin- $\frac{1}{2}$  XXZ-chain of length  $L = 40$  at  $\Delta = 0.8$ , time evolution in the Heisenberg picture. a) OSEE  $S^{[20]}(t)$  of  $\hat{P}_N \hat{\sigma}_{20}^z \hat{P}_N$  (solid,  $N = 1, 2, 4, 8, 16, 20$  from bottom up) and  $\hat{\sigma}_{20}^z$  (dashed: from canonical, crosses: from brute force calculation). Panels b) and c) both show the OSEE  $S^{[m]}(t)$  between sites  $m$  and  $m + 1$ . Initial operators are b)  $\hat{\sigma}_{20}^z$  (calculated using the unprojected method) and c)  $\hat{P}_{16} \hat{\sigma}_{20}^z \hat{P}_{16}$  (calculated using the projected method). The same data sets as in figure 3 are used.

previous calculations,<sup>28,29</sup> a decisive conclusion whether the transport is ballistic or diffusive can not be drawn.

We calculate the ITAC here to compare the power of the different methods discussed above. In figure 3 we show Heisenberg picture t-DMRG results for the normalised ITAC at  $\Delta = 0.8$  both in the grand canonical ensemble,

$$G(t) = \langle (\hat{\sigma}_m^z)_t \hat{\sigma}_m^z \rangle_{T=\infty} = \text{Tr} [(\hat{\sigma}_m^z)_t \hat{\sigma}_m^z] / 2^L, \quad (29)$$

as well as in the canonical ensemble,

$$C_N(t) = \langle (\hat{\sigma}_m^z)_t \hat{\sigma}_m^z \rangle_{T=\infty} = \text{Tr} \left[ \left( \hat{P}_N \hat{\sigma}_m^z \hat{P}_N \right)_t \hat{\sigma}_m^z \right] / \binom{L}{N}. \quad (30)$$

Because  $\text{Tr} \left[ \left( \hat{P}_M \hat{O} \hat{P}_N \right)_t \hat{O} \right] = \text{Tr} \left[ \hat{P}_M \hat{O}_t \hat{P}_N \hat{O} \right] = \text{Tr} \left[ \hat{O}_t \hat{P}_N \hat{O} \hat{P}_M \right]$  we can calculate the latter from both the projected, time-evolved or the unprojected, time-evolved  $\hat{\sigma}_m^z$ . The behaviour in the canonical ensemble is as expected: For low filling,  $C_N(t)$  decays only to a finite value. (From combinatorial arguments we find that  $1 - C_N(t) \leq 4N/L$ .) Therefore at half filling  $C_N(t)$  has to be smaller than  $G(t)$ , because the latter is the weighted average

$$G(t) = \frac{1}{2^L} \sum_{n=0}^N \binom{L}{n} C_n(t). \quad (31)$$

Figure 3 shows, that for low filling the projected approach is clearly superior. However for generic filling ( $N = L/2$  corresponds to a total magnetisation of 0) longer times can be reached with the grand-canonical algorithm. All curves shown are calculated using about the same computational resources. In order to propagate  $\hat{P}_N \hat{\sigma}_{20}^z \hat{P}_N$  for half filling up to the same point in time with the same accuracy as  $\hat{\sigma}_{20}^z$  an increase of computation time and memory by an order of magnitude would be required. The reason becomes apparent in figure 4a. The OSEE scales logarithmically both in the grand-canonical and the canonical picture for generic filling. This is expected from.<sup>19,20</sup> In fact the OSEE looks the same for both  $\hat{\sigma}_{20}^z$  and  $\hat{P}_N \hat{\sigma}_{20}^z \hat{P}_N$ , but the latter is shifted by the entanglement present in the initial MPO. The cut-off error in the algorithm therefore grows faster and the calculation breaks down earlier. In this example the higher bond dimension available for fixed particle number does not quite make up for this. Vice versa, to propagate  $\hat{\sigma}_{20}^z$  up to  $t = 20$ , as can be done easily for  $\hat{P}_N \hat{\sigma}_{20}^z \hat{P}_N$  for low filling, would also require an increase of computational resources by orders of magnitude.

The OSEE as a function of both lattice position and time is shown in figure 4b-c. The light cone like appearance is imposed by causality<sup>¶</sup>. It confirms that there will be no finite size effects in the centre of the trap before times close to 20. The projected operator is distinguished from the unprojected mainly by the fact, that there is initial entanglement away from the centre (which is where  $\hat{\sigma}_{20}^z$  acts nontrivial), compare to the illustration given in figure 1. It is constant in time, as  $|\hat{P}_N\rangle$  is an eigenstate of  $\tilde{H}$ . The entanglement generated dynamically merely adds.

Fig. 3 also shows a brute force calculation for  $G(t)$ , that does not take into account particle number conservation at all. It is clearly inferior to the unprojected method, section 2. Again a huge increase in computational resources would be required to reach the same accuracy.

As an additional example we take the Bose Hubbard model,

$$\hat{H} = -J \sum_{\langle m,n \rangle} (\hat{a}_m^\dagger \hat{a}_n + h.a.) + \frac{U}{2} \sum_m \hat{a}_m^\dagger \hat{a}_m^\dagger \hat{a}_m \hat{a}_m. \quad (32)$$

The  $\hat{a}^\dagger$  and  $\hat{a}$  operators are bosonic creation and annihilation operators. The first sum is again over nearest neighbours. For convenience, we set the hopping parameter  $J = 1$ . Recently there is a lot of interest in the thermalization of far-from equilibrium states (not only in this model). Cramer et al.<sup>31</sup> investigated the dynamics of the ‘‘anti-ferromagnetic’’ state  $|\Psi_0\rangle = |0101 \dots 0101\rangle$  using Schrödinger picture t-DMRG. They propose an experimental

¶ A more rigorous result of this reasoning is the well known area law.<sup>30</sup>

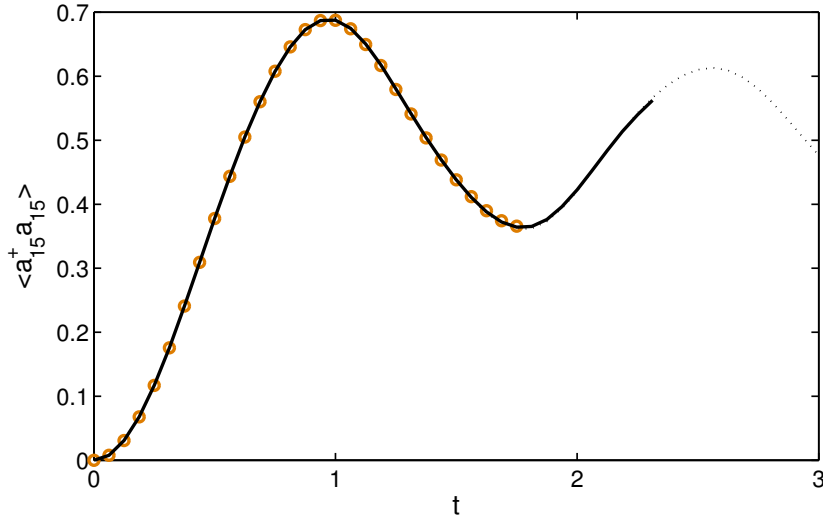


**Figure 5.** Expectation value of the local density at site 15 on a Bose Hubbard lattice (restricted to local dimension  $d = 4$ ) of length  $L = 30$  at  $U = 10$  initially prepared in the state  $|0101 \dots 0101\rangle$ , calculated using the projected (solid, black) and the unprojected method (orange circles). Bond dimensions used where  $\chi = 2000$  in the canonical calculations,  $\chi = 500$  in the grand canonical. Both curves end at the point where the accumulated cut-off error reaches  $10^{-3}$ . The dashed line shows the result of a Schrödinger picture calculation which can be regarded exact, as the cut-off error is numerically zero at this time scale. A TEBD<sup>4</sup> version of the t-DMRG algorithm is used with a fourth order trotter decomposition and time step size  $1/16$  in all three cases.

setup to prepare this state and observe its dynamics in an experiment using ultracold atoms in optical lattices. First measurements have been reported recently.<sup>32</sup>

Fig. 5 shows the dynamics of the local density at site  $m = 15$  in a system of total length  $L = 30$ . Again the size has been chosen large enough, such that there are no boundary effects arriving at the centre for the times shown. The figure shows the expectation value in the state  $|\Psi_0\rangle$  (where site 15 is empty) calculated using both the unprojected,  $\langle \Psi_0 | \left( \hat{a}_{15}^\dagger \hat{a}_{15} \right)_t | \Psi_0 \rangle$ , and the projected method,  $\langle \Psi_0 | \left( \hat{P}_{15} \hat{a}_{15}^\dagger \hat{a}_{15} \hat{P}_{15} \right)_t | \Psi_0 \rangle$ . Since  $|\Psi_0\rangle$  is a particle number eigenstate, both expectation values are identical and coincide with a Schrödinger picture calculation,  $\langle \Psi_0 |_t \hat{a}_{15}^\dagger \hat{a}_{15} | \Psi_0 \rangle_t$ .

Again both curves are calculated using approximately the same numerical resources. For performance purposes, we restrict the local Hilbert space to  $d = 4$ . We find that using the projected method we can calculate up to considerably larger times. So here the projected method is ahead of the unprojected, *even* if the particle number  $N$  is of the order of  $L/2$ , in contrast to the first example. While the projected method is only moderately affected by a higher local dimension  $d > 4$  ( $d = 16$  being the largest meaningful number here), the unprojected one breaks down as the Hilbert space dimension increases (not shown in the figure).

Although the timescales reachable are not large enough to see the local density equilibrate at  $\frac{1}{2}$ , a Schrödinger picture calculation is actually the method of choice in this example, as the timescale reachable is still significantly larger<sup>31</sup> than in the Heisenberg picture. This is true in spite of the fact, that the local density is a conserved density and in the Heisenberg picture we therefor expect much better scaling of the OSEE with time.<sup>20</sup> It can be explained by the overhead of having to include high local occupation numbers in the Heisenberg picture (in contrast to the above spin- $\frac{1}{2}$  example), which are actually not populated dynamically for the given initial state. In the case of a highly entangled or mixed state, the situation might be very different.

## 6. Conclusion

The two different approaches to include particle number conservation into an MPO have quite different effects on the performance of a Heisenberg-picture t-DMRG. The unprojected method brings the advantages known from ordinary (t-)DMRG, namely, the reduction of the Hilbert space dimension without introducing any additional entanglement. It is the method of choice in the presence of an appropriate symmetry. The Hilbert space dimension can be further reduced by projecting the MPO to a certain symmetry-sector. The effect then is quite counter-intuitive. Although the projected operators do only contain a small subset of the information present in the grand-canonical MPO, their propagation in time is not always easier. This is due to the entanglement introduced by fixing the total particle number. (Unity is not a product operator if projected to a symmetry sector.) In the low filling case, the reduction of the Hilbert space dimension is more important and we gain access to longer times. For generic filling however, the grand-canonical method remains superior.

## Acknowledgements

I am indebted to M. Fleischhauer for valuable discussions during the completion of this work.

## References

- [1] Kramers H A and Wannier G H 1941 *Phys. Rev.* **60** 263–276
- [2] Baxter R J 1978 *J. Stat. Phys.* **19** 461–478
- [3] White S R 1992 *Phys. Rev. Lett.* **69** 2863–2866
- [4] Vidal G 2003 *Phys. Rev. Lett.* **91** 147902
- [5] Vidal G 2004 *Phys. Rev. Lett.* **93** 040502
- [6] Daley A J, Kollath C, Schollwöck U and Vidal G 2004 *J. Stat. Mech.* P04005
- [7] White S R and Feiguin A E 2004 *Phys. Rev. Lett.* **93** 076401
- [8] McCulloch I P 2007 *J. Stat. Mech.* P10014
- [9] Schollwöck U 2011 *Ann. Phys. (New York)* **326** 96–192
- [10] Singh S, Zhou H Q and Vidal G 2010 *New J. Phys.* **12** 033029
- [11] Daley A J, Clark S R, Jaksch D and Zoller P 2005 *Phys. Rev. A* **72** 043618
- [12] Muth D, Schmidt B and Fleischhauer M 2010 *New J. Phys.* **12** 083065
- [13] Muth D and Fleischhauer M 2010 *Phys. Rev. Lett.* **105** 150403
- [14] Muth D, Fleischhauer M and Schmidt B 2010 *Phys. Rev. A* **82** 013602

- [15] Verstraete F, Garcia-Ripoll J J and Cirac J I 2004 *Phys. Rev. Lett.* **93** 207204
- [16] Zwolak M and Vidal G 2004 *Phys. Rev. Lett.* **93** 207205
- [17] Hartmann M J, Prior J, Clark S R and Plenio M B 2009 *Phys. Rev. Lett.* **102** 057202
- [18] Prosen T and Žnidarič M 2009 *J. Stat. Mech.* P02035
- [19] Prosen T and Žnidarič M 2007 *Phys. Rev. E* **75** 015202(R)
- [20] Muth D, Unanyan R G and Fleischhauer M 2011 *Phys. Rev. Lett.* **106** 077202
- [21] Perez-Garcia D, Verstraete F, Wolf M M and Cirac J I 2007 *Quant. Inf. Comp.* **7** 401–430
- [22] Verstraete F, Porras D and Cirac J I 2004 *Phys. Rev. Lett.* **93** 227205
- [23] Vidal G 2007 *Phys. Rev. Lett.* **98** 070201
- [24] Freund J E 1956 *Am. Math. Mon.* **63** 20–27
- [25] Calabrese P and Cardy J 2005 *J. Stat. Mech.* P04010
- [26] Verstraete F and Cirac J I 2006 *Phys. Rev. B* **73** 094423
- [27] Schuch N, Wolf M M, Verstraete F and Cirac J I 2008 *Phys. Rev. Lett.* **100** 030504
- [28] Fabricius K and McCoy B M 1998 *Phys. Rev. B* **57** 8340–8347
- [29] Sirker J 2006 *Phys. Rev. B* **73** 224424
- [30] Bravyi S, Hastings M B and Verstraete F 2006 *Phys. Rev. Lett.* **97** 050401
- [31] Cramer M, Flesch A, McCulloch I P, Schollwöck U and Eisert J 2008 *Phys. Rev. Lett.* **101** 063001
- [32] Trotzky S, Chen Y A, Flesch A, McCulloch I P, Schollwöck U, Eisert J and Bloch I 2011 (*Preprint* 1101.2659)